19th Brazilian Congress of Thermal Sciences and Engineering
November 6th–10th, 2022, Bento Gonçalves - RS - Brazil

ENC-2022-0229
PERMEABILITY PREDICTION OF KARST POROUS MEDIA USING CONVOLUTIONAL NEURAL NETWORKS

Gabriel Grenier Ferreira Motta
Monique Feitosa Dali
Sergio Santiago Ribeiro
Márcio da Silveira Carvalho
Mechanical Engineering Department, Pontifícia Universidade Católica do Rio de Janeiro, RJ 22451-900, Brazil
ggfmotta@hotmail.com; mfeitosa@lmmp.mec.puc-rio.br; sergio@lmmp.mec.puc-rio.br; msc@puc-rio.br

Abstract. *Averaging methods are widely used to estimate the average permeability of oil reservoirs. The Darcy Equation receives a measured flow, corresponding to an applied pressure differential, to obtain a good approximation of mean permeability. For media with homogeneous porous structure, it is possible to obtain a relationship between permeability and porosity of the media. However, karstified rock formations, such as carbonates, present vugs, fractures and other cavernous structures with abrupt variations in local porosity and permeability. Determining a good correlation between the patterns of karst structures and the generated increase in permeability would considerably increase the accuracy of heterogeneous reservoir characterization methods. Recently, convolutional neural networks (CNNs) have been used to estimate the effects of karst characteristics on the equivalent permeability of a porous carbonate medium, based on images of the macroporosity structures of the sample. The methodology continued from previous works consists in: (i) simulating the flow through a 2D mesh built on the basis of rock microtomography images using the Brinkman model; (ii) creation of a training database from the macroporosity binary images and the corresponding increase in simulated permeability in relation to the permeability of the rock matrix; (iii) finally the trained CNN is used to estimate the equivalent permeability increment of unseen porous karst media images. The present work re-implements this methodology in two-dimensional microtomography images obtained from Brazilian carbonate samples. In addition, it presents a comprehensive sensitivity analysis of the CNN architecture and training parameters with respect to the effective accuracy of the permeability prediction. Finally, the current study complements the previous study with an assessment of CNN's ability to generalize patterns learned from an image-specific training dataset. The analysis evaluates which network characteristics allow to reasonably predict the permeability increments within a test dataset composed of unseen rock samples with different permeability ranges from the training ones. Although the main goal could not be achieved, the observations made during the analyses indicate that CNNs are capable of predicting permeability increase due to karstic structures, trained with images of similar and restricted permeability range.*

Keywords: *machine learning, equivalent permeability, reservoir characterization, karst porous medium*

1. INTRODUCTION

1.1 Problem Description

The permeability of a porous medium is the most important property in the characterization of oil and gas reservoirs, and it is a function of the effective porosity of the medium and the connectivity and shape of its pores. That said, in a homogeneous porous medium, with pores of similar sizes, well-distributed dispersion and a porous matrix uniformly connected, the greater its porosity, the greater the permeability of that medium.

However, in some types of rock, such as carbonates, the pore geometry can present large variations in scale. Such porous media presents caves and vugs much larger than the rock matrix pores, usually referred as karsts (Rosa *et al.*, 2006; Glossary, 2020). Due to its heterogeneity, an equivalent permeability is normally defined to incorporate the effects of these macro-porosities on average flow methods. Therefore, determining the equivalent permeability can be a very complex task.

1.2 Motivation

A major challenge, in carbonate reservoirs such as Brazilian pre-salt, is to precisely increase the scanning efficiency. The high heterogeneity of these rocks (Oliveira and Carvalho, 2014) is a factor that intensifies the creation of preferential flow paths for the injected fluid, leaving pockets of oil behind during production.

Knowing the permeability of different reservoir regions is of fundamental importance to define the best production strategy. Therefore, accurate and fast predictions of karstic porous media permeability are extremely valuable for the industry. As in other areas of knowledge, combining fluid mechanics with computational intelligence has proven to be a very powerful tool and will be a trend in the coming years (Zaparolly, 2021).

1.3 Objective

The present work aims to combine the methods already used in the study of fluid mechanics in heterogeneous porous media with computational intelligence algorithms used to estimate permeability in karstified media. Computational Intelligence algorithms have been increasingly used to solve engineering problems, mainly replacing traditional techniques of higher computational cost, such as the different methods of computational fluid dynamics (CFD).

From the implementation of deep learning techniques, it becomes possible to understand the relationship of the model's input parameters with the correspondent answers given. In this case, a Convolutional Neural Network (CNN) will receive a large amount of binary macroporosity images as inputs and the respective equivalent simulated permeabilities as a targets, mapping the correlation of various aspects of each image with the magnitude of the corresponding target. Finally, it is expected that this network will be able to infer the effective permeability of the porous media analyzed, coming from images never seen before by the network, with a high level of reliability.

2. THEORETICAL BACKGROUND

2.1 Heterogeneous Porous Media

Karstic porous media show great heterogeneity in the geometric scale of their pores, presenting great variations in the scale of their pores along the reservoir (Rosa *et al.*, 2006). Therefore, some authors tend to treat a heterogeneous porous medium as the combination of a homogeneous rocky matrix with pores on the micrometric scale and a network of larger pores, of different geometries, sizes and connections (Rosa *et al.*, 2006)

Figure 1 presents a 2D binary micro-tomography image of a carbonate rock sample. The presence of different pore structures and interconnections can be observed, represented in black, and the white spaces around it represent the rocky matrix, which has pores at much smaller scales, not visible in the image resolution.

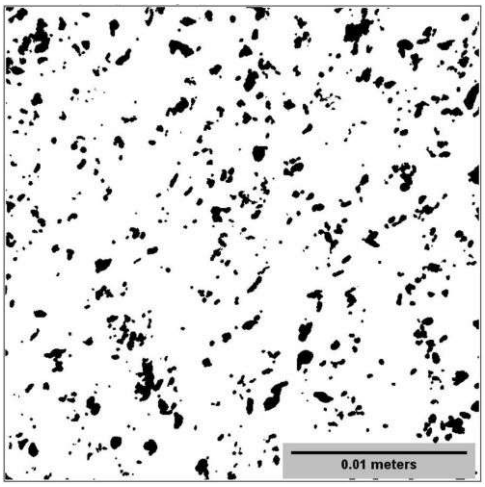

Figure 1. Microtomografy binary capture of carbonatic rock. Example of heterogeneous media. (Dali *et al.*, 2019)

An important property of the porous medium is the porosity ϕ, calculated as the ratio between the macro-pore volume V_{pores} and the total sample volume V_{total}, as shown in Eq. 1.

$$\phi = \frac{V_{pores}}{V_{total}} \tag{1}$$

In karstic reservoir, the total sample porosity is a combination of rock matrix porosity (micro pores) and karsts (macro pores).

2.2 Conservation Equations

To deal with the different pore scales, a combined approach is usually applied. The Stokes equation governs the flow of fluids in porous spaces and Darcy equation governs the average flow in the rock matrix. Assuming incompressible flow with constant viscosity(μ), the momentum and mass conservation equations are simplified in imcompressible Navier-Stokes equations, written in vector form in Eq. 2.

$$\rho\left(\frac{\partial\vec{V}}{\partial t}+\vec{V}\cdot(\nabla\cdot\vec{V})\right)=\rho g-\nabla P+\mu\nabla^2\vec{V} \tag{2}$$

, where $\vec{V}$ is the velocity field, P is the pressure field, t is the time, g is the gravity acceleration, and ρ is the fluid density. According to Fox *et al.* (2001), for steady state flows the time variant term is deleted. In addition, and at low Reynolds numbers, the inertia term can be neglected and the Navier-Stokes equations are simplified to the Stokes equation, showed in Eq. 3.

$$\rho g+\mu\nabla^2\vec{V}=\nabla P \tag{3}$$

2.3 Darcy Equation

The Darcy's law is chosen as the method of average transmissibility to predict average flow inside the rock matrix (Oliveira and Carvalho, 2014). As shown by Eq. 4, it establishes that the flowrate Q is directly proportional to the pressure gradient ∇P, the sample cross section area A and the constant permeability of the rock matrix k, and inversely proportional to the fluid viscosity μ.

$$\frac{Q}{A}=-\frac{k}{\mu}\nabla P \tag{4}$$

2.4 Brinkman Model

The Brinkman model combines the Darcy and Stokes equations through a single differential equation, as presented in Eq. 5. It is widely used to model rocks in which the pore size scale varies from micrometric pores to large faults and caves. In those karst geometries the fluid flows freely at high speeds when compared with those in rock matrix, as seen in Oliveira and Carvalho (2014).

$$\nabla P=-\frac{\mu}{k}\vec{V}+\mu^\star\nabla^2\vec{V} \tag{5}$$

In the rocky matrix, containing small pores, where the flow obeys Darcy's Law (Eq. 4), μ^* is set to zero, neglecting the Stokes part. In the space constituted by the macroscopic pores, where the flow obeys the Stokes equation (Eq.3), the permeability k is set to infinity, in order to turn off the Darcy term. That said, the Brinkman model can be understood as a single equation capable of representing the fluid flow in two different domains.

Using the Brinkman equation and the finite element model, Dali *et al.* (2019) solved the system of differential equations that describes a two-dimensional flow through a porous medium with macro pores. The objective of its analysis was to evaluate an equivalent permeability as a function of the area and structure of the macro pores, giving as input 2D slices of tomographic images of different types of rocks. However, these numerical flow simulations still present a high computational cost, considering a life-size sample. This makes the determination of the equivalent permeability of heterogeneous media by this methodology quite expensive.

As seen in Marcato *et al.* (2021), the data-oriented models are able to understand the relationships that intervene between the input features for the prediction of output parameters with significant speed gain, making it a valid alternative to traditional models based on physical. According to the authors, these types of models were coupled to CFD models to predict the properties of fluid dynamics. As in flow problems in porous media, where most of the time it is a challenging scenario.

2.5 Convolutional Neural Networks (CNN)

According to Nielsen (2015), convolutional neural networks can be described as Deep Learning algorithms that have particularly ideal architectures for solving image identification problems. Such architectures make use of three basic concepts: local receptive fields, shared weights and biases, and clustering layers.

Nielsen (2015) defines the convolutional network structure as showed in 2. It starts with an input layer with local receptive fields of predefined size, therefore a small window in the image pixels. This window's main function is to establish a connection with a hidden neuron layer, called convolutional layers. In addition, multiple resource maps are

defined by a set of shared weights and a single shared bias. The Pooling layers are used to simplify the information in the output a convolutional layer into the next one. Finally the fully connected layers of neurons connects the convolutional part to the output layer, which is responsible for model prediction.

The number of hidden layers and clustering layers varies according to the objectives of each problem, and consequently, many of the parameters are empirically determined. Therefore, to determine these parameters is in the scope of this project.

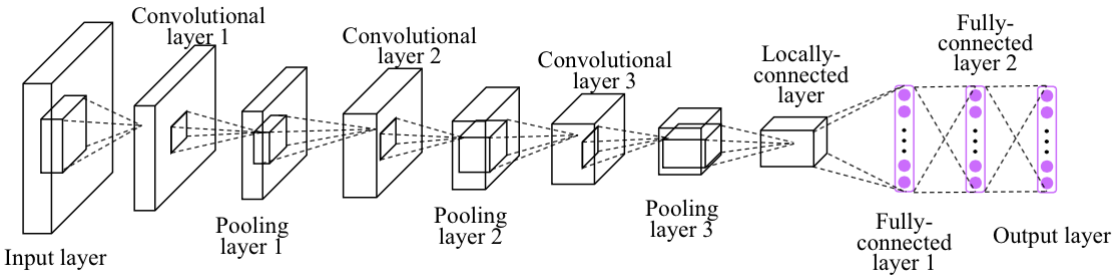

Figure 2. Example of the final architecture of a CNN (Nielsen, 2015)

According to Brownlee (2016), the hidden layers of a single model usually make use of the same activation function. And, according to the author, for CNN-like networks, this should be the Rectified Linear (ReLu) activation function. Due to its effectiveness, practicality and simplicity of implementation. As for the output layers, in CNN-like networks, Brownlee (2016) recommends the use of the Linear activation function, as this is mainly a regression problem.

3. METHODOLOGY

3.1 Input Data Generation

An image database was made available from micro tomography of two carbonate rock plugs by the Laboratory of Micro Hydrodynamics in Porous Media (LMMP), at PUC-Rio. The images were obtained during the work of Dali *et al.* (2019), and are the result of a digital processing of the entire plug that divides it into 2D slices. Therefore, the generation of input data was divided into two stages, described below.

3.1.1 Porous media image segmentation

Initially, the macro pores present in the micro tomography images of the analyzed rocks need to be identified. The images of porous media were segmented, using the OpenCV library in Python language, and the binary images are obtained. On the following, the contours of vugs and macropores are extracted from these segmented images. Subsequently, two-dimensional meshes are generated with two different domains each, separated by the extracted contours. The open Source library pyGmsh, also in the Python language, is used to create the triangular meshed, as showed in Figure 3.

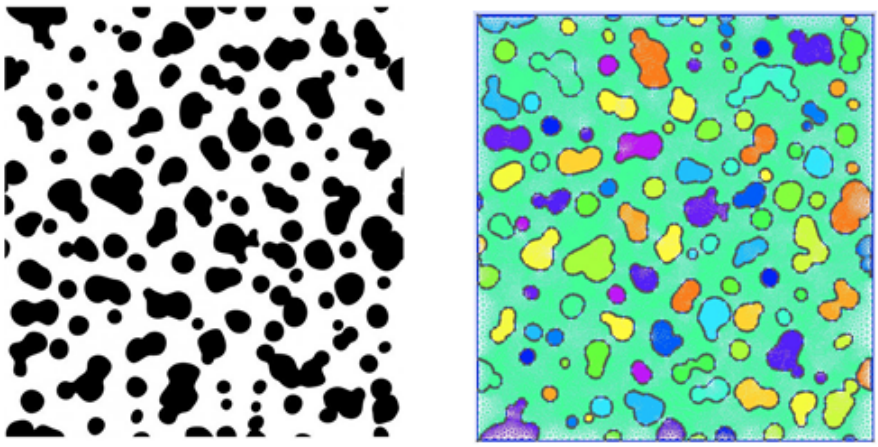

Figure 3. Example of segmentation and mesh generation (right) of a topographical image of a porous medium (left).

According to the methodology presented by Dali *et al.* (2019), the Brinkman model (Eq. 5) is applied to both discretized domains that composes the mesh, rock matrix and pore spaces.

3.2 Brinkman Model Implementation

With the porous media images properly segmented, the output mesh is used to obtain the steady-state flow though the pores, under a certain pressure difference condition. The Brinkman equation is solved using the finite elements method, implemented in python using the open source numerical library Dolfin(Logg *et al.*, 2012).

The imposed pressure gradient was defined, so that low Reynolds numbers are respected. The outlet flow rate obtained is used to calculate an increased effective permeability with respect to the rock matrix permeability, incorporating the macro pores flow contribution.

In Figure 4 its possible to observe the behavior of the pressure and velocity fields, respectively. The imposed pressure difference applied is from bottom to top boundaries of the domain. As expected, the segmented mesh used for this example is shown in Figure 3, and the pores coincide with observed discontinuities in the pressure field. Outside the pores, the pressure drop is smoother, since the rock matrix permeability is assumed constant.

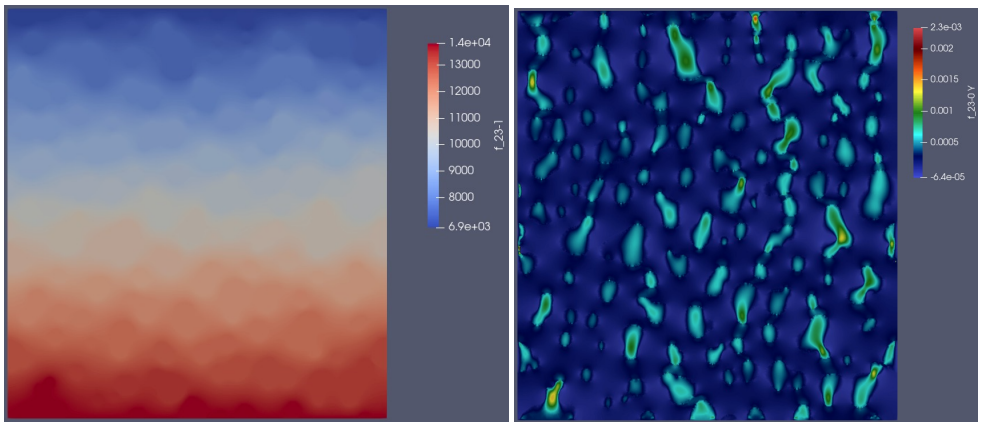

Figure 4. Example of pressure profile (left) and velocity magnitude (right) through a 2D porous media.

The rock macro pores and vugs present greater velocity gradients than the rock matrix, about 100 times greater. These extremely low velocity magnitudes observed in the rock matrix were also expected, since the permeability is much lower than within the pores. These simulations are then executed to all images, generating a vast database with images associated with equivalent permeability increments. This samples of input-output pairs are then used to train the Neural Networks training algorithm.

The images originated from two different rock samples, named “Am5” and “Am8”, relative to the sample orientation with respect to the reservoir. Each sample has a certain range of pore sizes and aggregated structures. In order to enhance the number of images used to train the neural network, each image of those two samples were digitally eroded with four different intensities, generating four extra subdivisions on the data, named types as C1, C2, C3 and C4.

Figure 5 exemplify the difference between images of different groups used for this study. In these images, the black region represents the macropores and the white region, the porous matrix, which has known permeability.

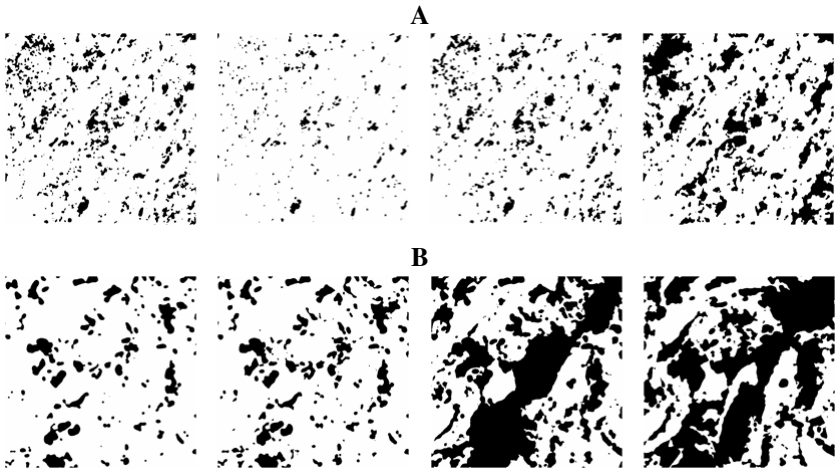

Figure 5. Image examples from "Am5" (A) and "Am8" (B) samples, from left to right of subdivisions C1, C2, C3 and C4.

3.3 CNN architecture development

In order to evaluate the Neural Network capacity of generalization, it was decided to group the most similar subdivisions of each different sample. Thus, the images can be redivided in 4 new groups: 1) C1 and C2 of the Am5 sample; 2) C3 and C4 of the Am5 sample; 3) type C1 and C2 of the Am8 sample; 4) type C3 and C4 of the Am8 sample. This new groups increase the number of images available for training, and could only be formed after the initial screening tests showed permeability similarities among the images of each group.

A test matrix was defined, as shown in Table 1. The objective is to find an optimal CNN architecture from the empirical variation of some topology and training parameters. Related to the network topology: Kernel Size, which is the number of convolutional neurons; Stride and Pool Sizes, which are the convolution and pooling layer window sizes respectively. Related to training, the parameters that can influence generalization (Abadi *et al.*, 2016) are: Batch Size, which is the number of samples per training iteration; Split Size, which is the proportion by which the input data set is divided into training data and test data; and Epochs, which is the total of training iterations.

Table 1. Different model topologies that will be tested

Model Topology	Kernel size	Stride	Pool size	Batch size	Split size	Epochs
1	256	(5; 5)	(2; 2)	10	0.15	10
	128	(3; 3)	(2; 2)			
	64	(3; 3)	(2; 2)			
2	256	(5; 5)	(2; 2)	10	0.15	20
	128	(3; 3)	(2; 2)			
	64	(3; 3)	(2; 2)			
3	256	(5; 5)	(2; 2)	50	0.15	20
	128	(3; 3)	(2; 2)			
	64	(3; 3)	(2; 2)			
4	256	(7; 7)	(2; 2)	10	0.15	20
	128	(5; 5)	(2; 2)			
	64	(5; 5)	(2; 2)			
5	384	(5; 5)	(2; 2)	10	0.15	20
	192	(3; 3)	(2; 2)			
	96	(3; 3)	(2; 2)			
6	512	(5; 5)	(2; 2)	10	0.15	20
	256	(3; 3)	(2; 2)			
	128	(3; 3)	(2; 2)			
	64	(3; 3)	(2; 2)			

4. RESULTS

4.1 Choosing the optimal CNN topology

The performance of the topologies established in the test matrix, defined in Section 3.3, can be seen in Table 2. From these values, it can be concluded that the topology with the best performance was Topology 2, which presented the lowest standard deviation, both for training data and for test data. Followed by Topology 6 which also presented a very satisfactory performance, although it has a higher standard deviation for the training data than Topology 5, because what really counts is the performance for the test data. However, it is important to point out that Topology 6 took about 4 h longer to finish its training and predict the results than the best performing topology, which is due to the greater number of convolution layers in its architecture.

The poor performance of Topology 1 is easily explained by the amount of epochs of only 10 units in its architecture. Note that only this parameter was responsible for such a difference between this and Topology 2, the one with the best performance. Topology 3, on the other hand, achieved a performance far from the desired, exclusively due to the batch size value of its architecture, which is the only parameter that differentiates it from the topology with the best result. Finally, the lower-than-desired performance of Topology 4 is due to the increase in the Stride layer, since large values in this parameter end up oversimplifying some characteristics of the input images and, consequently, making it difficult to learn the network.

For a better view, Figure 6 and Figure 7 show the correlation of the results of each set of groups tested just below each table. In Figure 6 it is possible to observe the dispersion of the estimated equivalent permeability with the theoretical one. In Figure 7, it is possible to observe the dispersion between the relative error in module with the theoretical equivalent

Table 2. Results per sample, type and dataset

Topology	Training			Test		
	Mean Error (%)	Max. Error (%)	Standard Deviation (%)	Mean Error (%)	Max. Error (%)	Standard Deviation (%)
1	2.458	5.709	1.034	2.430	7.200	1.040
2	0.821	3.548	0.630	0.826	4.010	0.635
3	1.473	5.813	1.158	1.430	6.260	1.110
4	3.156	6.389	1.093	3.190	6.450	1.030
5	1.609	3.814	0.771	1.610	4.450	0.755
6	0.985	4.927	0.777	0.964	4.360	0.729

permeability.

It is interesting to note that the best performing topologies (Topologies 2 and 6) presented significantly higher relative errors for the highest equivalent permeabilities, around 1.15 [-], although, in general, both present an average error around 1.0%-symbol, which is excellent and can be interpreted as extremely reliable. The other topologies, on the other hand, showed a much more significant dispersion in their results, both for lower equivalent permeabilities, around 1.0 [-], and for those with higher values, reflecting a considerably higher average error.

It is important to note that, in the scatter plots shown in Figure 6, between the theoretical equivalent permeability and that predicted by the tested neural network configuration, the line drawn along the graph has an inclination equivalent to 45°, as it indicates the value that the permeability equivalent predicted by the network should have, that is, equal to the theoretical permeability.

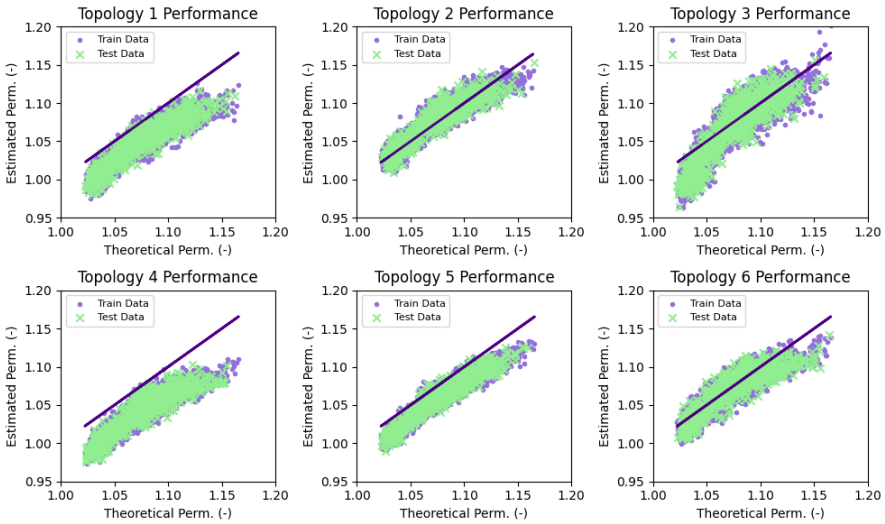

Figure 6. Scatter plots between the estimated and theoretical equivalent permeability of each topology tested for the group of images Am5 and types C1 and C2.

4.2 Optimal topology on the other remaining groups

Once Topology 2 was established as the optimal topology, it then started to test it in the other groups not studied. They are the group Am5 with types C3 and C4, the group Am8 with types C1 and C2 and the group Am8 with types C3 and C4. The performance of the models is shown in Table 3.

From these results, it was possible to observe that the network performed satisfactorily for the first and second groups of images, where in both cases a standard deviation of around 2.00%-symbol was presented. It is important to emphasize that in these two cases the equivalent permeabilities can still be considered low, although relatively higher than when compared with the Am5 group and types C1 and C2. Even in the group of images Am5 and types C3 and C4, where the permeabilities reach values in the order of 2.00 [-], the network ended up performing better than when trained for images of the group Am8 and types C1 and C2. Therefore, it can be concluded that, in general, learning was better for Am5 images.

However, the network learning for the group of images Am8 and types C3 and C4 can be considered unsatisfactory, given the values of the metric parameters shown in Table 4. This is better understood when analyzing the dispersion of

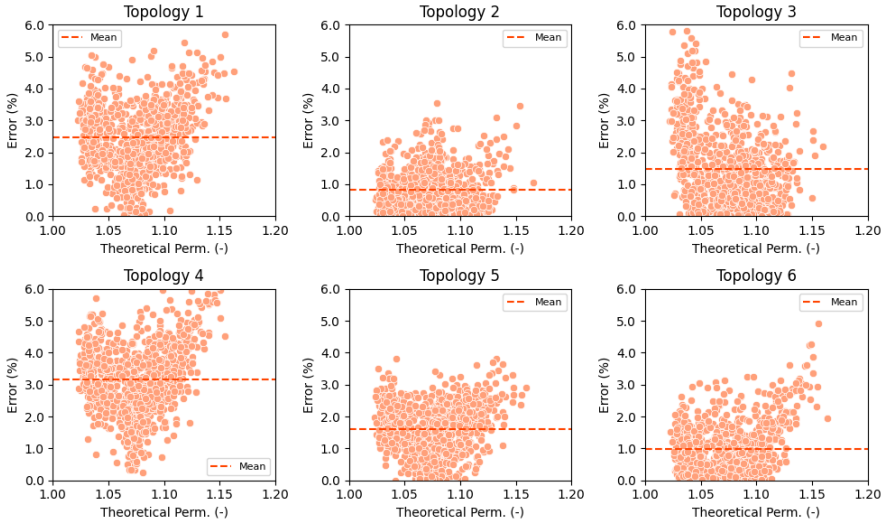

Figure 7. Scatter plots between the relative error obtained and the theoretical equivalent permeability of each tested topology.

Table 3. Results per sample, type and dataset

Samples	Types		Topology	Training			Test		
				Mean Error (%)	Max. Error (%)	Standard Deviation (%)	Mean Error (%)	Max. Error (%)	Standard Deviation (%)
5	3	4	2	2.35	13.7	1.96	2.54	58.11	2.84
8	1	2	2	3.24	16.00	2.36	3.23	15.60	2.22
8	3	4	2	92.00	582.00	88.60	97.50	555.50	93.89

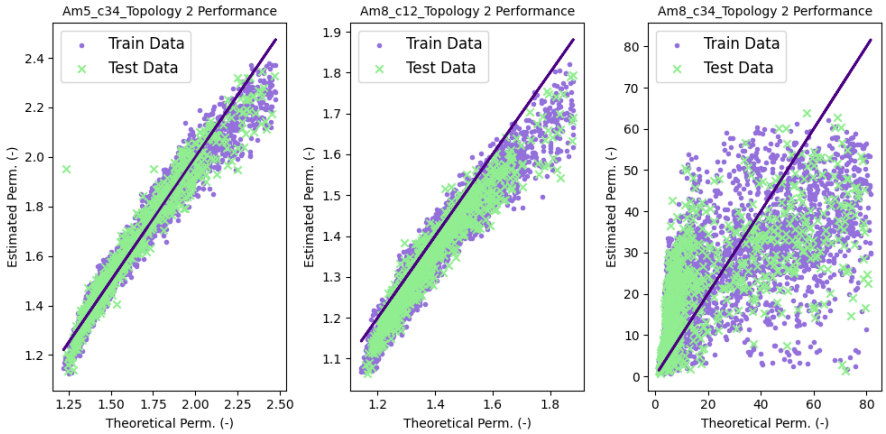

Figure 8. Scatter plots between the estimated and theoretical equivalent permeability of each topology tested for the remaining groups: Am5 and types C3 and C4; Am8 and types C1 and C2; Am8 and types C3 and C4.

the data in Figure 8. In the image, it is noted that in this group of images, there are images with equivalent permeabilities even in the order of 80.0 [-], while there are images with permeabilities about eighty times smaller than that. That said, it can be concluded that the assumed permeability range directly impacts the learning of the network, that is, the larger it is, the more the group will need more robust training.

4.3 Special training

Considering that the range of values assumed for the sample group Am8 and types C3 and C4 is equivalent to 80.20 [-], it can be understood that this set ends up being quite generalized. Thus, in order to develop a CNN architecture capable of predicting the equivalent permeability of this group of images, it is believed that, in the end, there will be a

neural network capable of predicting the equivalent permeability of any image. Thus, adopting the same methodology as in the previous sections, a new test matrix was schematized, shown below in Table 4. The best performance architecture previously seen, Topology 2, was taken into account.

Table 4. Model Parameters by Topology

Model Topology	Kernel size	Stride	Pool size	Batch size	Split size	Epochs
2	256	(5; 5)	(2; 2)	10	0.15	20
	128	(3; 3)	(2; 2)			
	64	(3; 3)	(2; 2)			
2a	256	(5; 5)	(2; 2)	10	0.15	100
	128	(3; 3)	(2; 2)			
	64	(3; 3)	(2; 2)			
2b	256	(5; 5)	(2; 2)	10	0.15	500
	128	(3; 3)	(2; 2)			
	64	(3; 3)	(2; 2)			

For the definition of the parameters of the topologies, it was also taken into account that, considering that this time the equivalent permeabilities of all the images of the analyzed set are significantly more dispersed, the neural network will demand much more effort in its learning. As a result, the tactic of a gradual increase in the number of epochs was adopted, as can be seen in Table 4, aiming at minimizing the Loss function of the model, which is a simple "Mean Square Error", widely used in this type of problem.

Thus, in Figure 9, it is possible to observe the performance of the model and how the neural network learning grows as it is exposed to a greater number of epochs. Note that the greater the number of epochs, the smaller the loss function of the model. And, as in the previous sections, you can see the performance of each topology based on more metric parameters through Table 5.

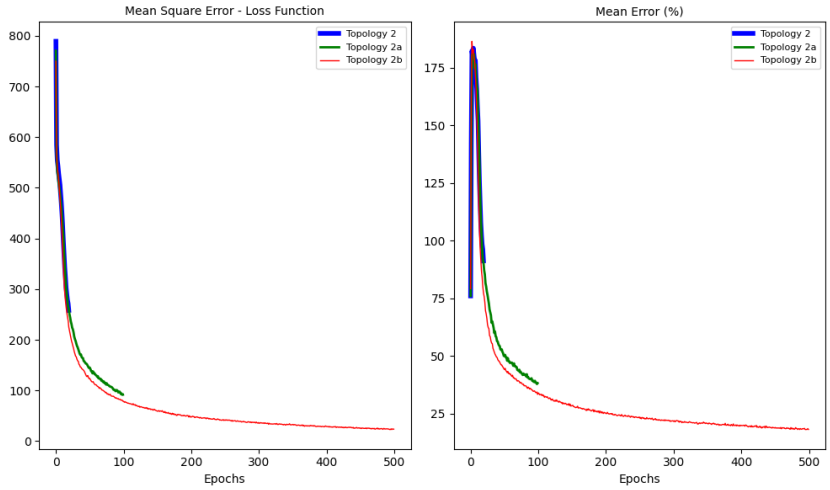

Figure 9. Special training performance. Loss Function graph on the left and correlation of the model's mean error with its number of epochs.

Table 5. Results by Topology and Dataset

Topology	Training			Test		
	Mean Error (%)	Max. Error (%)	Standard Deviation (%)	Mean Error (%)	Max. Error (%)	Standard Deviation (%)
2	92.00	582.00	88.60	97.50	555.50	93.89
2a	38.29	380.94	41.30	40.57	438.07	47.95
2b	15.20	216.00	20.10	21.38	260.60	28.48

It is worth mentioning that throughout the training, the early stopping technique was used, with the goal of minimizing the loss function of the model for a maximum interval of 50 epochs, that is, if its performance does not improve in this

interval, the training is interrupted. Thus, the model was interrupted at epoch number 496, and it can be concluded that with the other parameters of its architecture, it would not present a better performance in a greater number of epochs. Figure 10 shows the dispersion between the theoretical equivalent permeability and the one estimated by the best performing topology of this training section, Topology 2b.

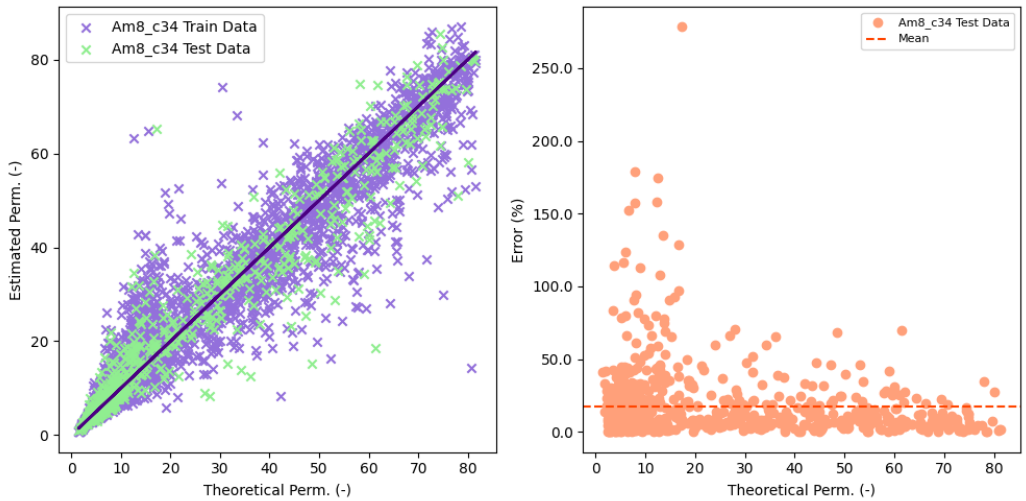

Figure 10. Scatter plot between the theoretical equivalent permeability and the one estimated by Topology 2b (left) and the dispersion of the relative error of each prediction with the theoretical equivalent permeability, for the group of images of the sample Am8 and types C3 and C4.

When observing the figure 10, it is noted that the final performance of this training cannot be considered satisfactory, mainly because 75%-symbol of the data used for the training of this neural network are below theoretical equivalent permeabilities equal to 35.84 [-].

It is also necessary to emphasize the importance of analyzing the performance of the model by the relative error, instead of the absolute error, because when observing Figure 10, one can hastily conclude that it presented a better performance for the images whose equivalent permeability has a considerably higher value. However, this could not be more false, since the same absolute error is relatively more significant for lower permeability ranges, which is precisely what should be observed in Figure 10. Therefore, even with images of lower equivalent permeability and with considerably high relative errors in their prediction, there are also images of low equivalent permeability with small relative errors in their predictions.

In this way, it can be concluded that the training performed was not able to deliver a neural network capable of generalizing different images with the most varied equivalent permeabilities with the desired reliability index.

4.4 Cross predictions

As the next step of the work, it was decided to test the capacity of the trained models with never-before-seen images of subgroups different from the one used for the training set. For this, the three models analyzed in the previous sections were used. The best model was then trained with images from Am5 sample and types c1 and c2, and tested with types c3 and c4. The original train and test chart(top left) is compared with the cross prediction tests(top right chart), as seen in Figure 11. The bottom charts show correspondent percentile test errors, by permeability ranges.

By analyzing Figure 11, it is possible to conclude that the performance was unsatisfactory. However, this was already expected, since the model training was based on images with slightly lower equivalent permeabilities. It is important to note that the lowest equivalent permeability of the subgroup formed by images from the sample Am5 and types C3 and C4 is greater than the highest equivalent permeability already seen by the model, which was trained with images from the subgroup formed by the sample Am5 and types C1 and C2. That said, the model does not know what are images with permeabilities greater than 1.16 [-] and, therefore, the prediction of this type of data with a high precision can be classified as very unlikely.

The second model analyzed here also has its architecture described by Topology 2 (Table 1), but it was trained using the subgroup of sample Am5, types C3 and C4. This time, to further test the performance of this model, we used the subgroup of images formed by the sample Am8 and types C1 and C2. This choice is justified by the intersection of the equivalent permeability ranges of both groups. Therefore, the aim is to analyze the model's ability to predict never-before-seen images, but which, in theory, it is capable of predicting. The forecast results can be seen in Figure 12, just below.

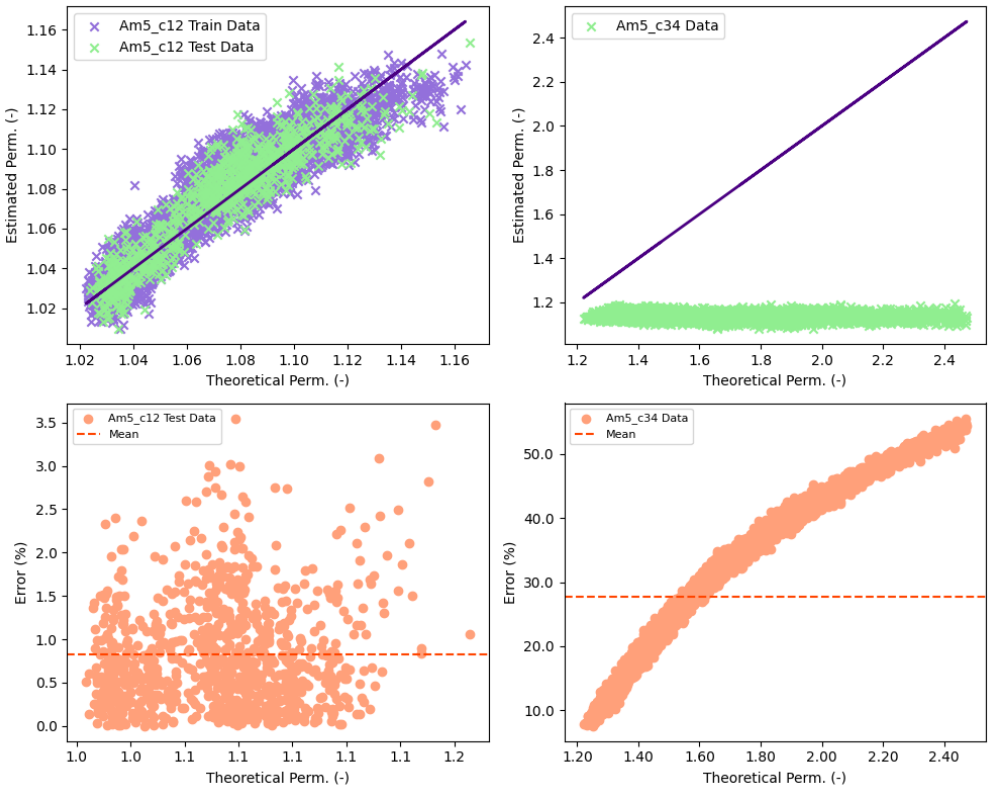

Figure 11. Use of the model trained with Topology 2, from images of the sample subgroup Am5 and types C1 and C2, to predict the equivalent permeabilities of images of the subgroup of the sample Am5 and types C3 and C4.

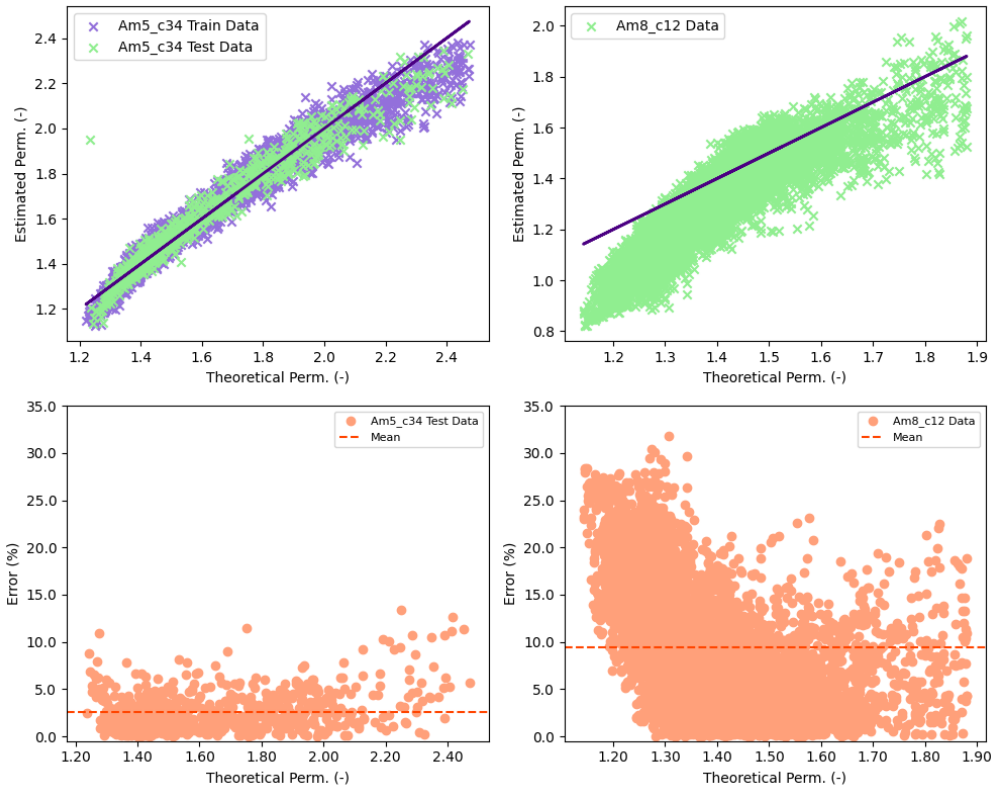

Figure 12. Use of the model trained with Topology 2, from images of the subgroup of the sample Am5 and types C3 and c4, to predict the equivalent permeabilities of images of the subgroup of the sample Am8 and types C1 and C2.

When analyzing Figure 12, it is possible to observe a higher level of accuracy in the predictions of equivalent permeabilities of the images of the sample subgroup Am8 and types C1 and C2 for the range of permeability values that are also present in the training data. Therefore, for images whose permeability is less than 1.20 [-], which is the lowest value seen during model training, it is possible to see that the relative error tends to be much higher. However, even though it was possible to observe a good correlation, a higher accuracy rate was expected, considering the tested permeability values are closer to the trained permeability range.

5. CONCLUSION

The initial objective of the work to build a general neural network capable of predicting the equivalent permeability based simply tomographic image of a 2D porous medium never seen before with high precision. Although this could not be achieved, from the observations made during the analyses, it is possible to draw some interesting conclusions about this topic.

It was observed that neural network models were able to accurately predict the equivalent permeabilities if it has been trained with images of similar and restricted permeability range. The models obtained in this work were not be able to predict the equivalent permeability, based purely on images, if those new images presented permeability ranges outside the trained ranges.

However, it is important to emphasize that, for a certain range of permeabilities, it was demonstrated in that it is possible to train neural network models capable of predicting it accurately, and that it does not require much computational effort. Considering that the training was carried out with only 20 epochs, according to Topology 2, in Table 1.

Regarding the observations made, it was possible to conclude that the greater the range of values assumed for the images used in a training set, the greater the computational effort required for training the neural network. Neither using the same successful topology of previous cases, nor with a training number of epochs considerably higher, it was possible to match the same results obtained for image sets within narrow permeability ranges.

Finally, it should also be noted that the model trained from a set of images of the most varied equivalent permeabilities also presented the same problem in predicting the permeability of never-before-seen images whose permeability does not resemble those of training.

That said, it is recommended for future work that, instead of aiming to build a single neural network model capable of predicting the equivalent permeability of any image, to seek to develop models that act in specific permeability ranges. Dividing the training data group not exclusively by the characteristics of the tomographic images, but by permeability intervals, and possibly training a classification neural network model to pre-categorize them. It is believed that in this way the training computational effort will be lower and the final result may be capable of predicting the results with a high level of precision, as initially desired in this work.

6. REFERENCES

Abadi, M., Agarwal, A., Barham, P., Brevdo, E., Chen, Z., Citro, C., Corrado, G.S., Davis, A., Dean, J., Devin, M. *et al.*, 2016. "Tensorflow: Large-scale machine learning on heterogeneous distributed systems". *arXiv preprint arXiv:1603.04467*.

Brownlee, J., 2016. *Deep learning with Python: develop deep learning models on Theano and TensorFlow using Keras*. Machine Learning Mastery.

Dali, M., Gomes, F. and Carvalho, M., 2019. "Equivalent permeability in vuggy porous media using brinkman's model". In *25th ABCM International Congress of Mechanical Engineering*. ABCM, pp. 1–10.

Fox, R.W., McDonald, A.T. and Pritchard, P., 2001. *Introdução à Mecânica dos Fluidos, 5ª edição*.

Glossary, S.O., 2020. "Oilfield glossary".

Logg, A., Mardal, K.A. and Wells, G., 2012. *Automated solution of differential equations by the finite element method: The FEniCS book*, Vol. 84. Springer Science & Business Media.

Marcato, A., Boccardo, G. and Marchisio, D., 2021. "A computational workflow to study particle transport and filtration in porous media: Coupling cfd and deep learning".

Nielsen, M.A., 2015. *Neural networks and deep learning*, Vol. 25. Determination press San Francisco, CA, USA.

Oliveira, R. and Carvalho, M., 2014. "Finite element method applied to flow in heterogeneous porous media". *Departamento de Engenharia Mecânica. Pontifícia Universidade Católica do Rio de Janeiro*.

Rosa, A.J., de Souza Carvalho, R. and Xavier, J.A.D., 2006. *Engenharia de reservatorios de petroleo*. Editora Interfẽncia.

Zaparolly, D., 2021. "Produção mais eficaz no pré-sal." `https://revistapesquisa.fapesp.br/`. Accessed: 2022-01-09.

7. RESPONSIBILITY NOTICE

The author(s) is (are) solely responsible for the printed material included in this paper.